New Journal of Physics
The open access journal at the forefront of physics

Deutsche Physikalische Gesellschaft DPG IOP Institute of Physics

PAPER • OPEN ACCESS

On the effectiveness of the collapse in the Diósi–Penrose model

To cite this article: Laria Figurato *et al* 2024 *New J. Phys.* **26** 113004

IOP Publishing New J. Phys. 26 (2024) 113004 https://doi.org/10.1088/1367-2630/ad8c77

New Journal of Physics
The open access journal at the forefront of physics

Deutsche Physikalische Gesellschaft DPG
IOP Institute of Physics

Published in partnership with: Deutsche Physikalische Gesellschaft and the Institute of Physics

OPEN ACCESS

RECEIVED
22 July 2024

REVISED
14 October 2024

ACCEPTED FOR PUBLICATION
29 October 2024

PUBLISHED
11 November 2024

PAPER

On the effectiveness of the collapse in the Diósi–Penrose model

Laria Figurato[1,2,4,*], **Marco Dirindin**[1,4], **José Luis Gaona-Reyes**[1,2], **Matteo Carlesso**[1,2], **Angelo Bassi**[1,2] and **Sandro Donadi**[2,3,*]

[1] Department of Physics, University of Trieste, Strada Costiera 11, 34151 Trieste, Italy
[2] Trieste section, Istituto Nazionale di Fisica Nucleare, Via Valerio 2, 34127 Trieste, Italy
[3] Centre for Quantum Materials and Technologies, School of Mathematics and Physics, Queens University, Belfast BT7 1NN, United Kingdom
[4] These authors contributed equally.
[*] Authors to whom any correspondence should be addressed.

E-mail: laria.figurato@phd.units.it and s.donadi@qub.ac.uk

Keywords: collapse models, measurement problem, quantum foundations, quantum measurements

Abstract

The possibility that gravity plays a role in the collapse of the quantum wave function has been considered in the literature, and it is of relevance not only because it would provide a solution to the measurement problem in quantum theory, but also because it would give a new and unexpected twist to the search for a unified theory of quantum and gravitational phenomena, possibly overcoming the current impasse. The Diósi–Penrose model is the most popular incarnation of this idea. It predicts a progressive breakdown of quantum superpositions when the mass of the system increases; as such, it is susceptible to experimental verification. Current experiments set a lower bound $R_0 \gtrsim 4\,\text{Å}$ for the free parameter of the model, excluding some versions of it. In this work we search for an upper bound, coming from the request that the collapse is effective enough to guarantee classicality at the macroscopic scale: we find out that not all macroscopic systems collapse effectively. If one relaxes this request, a reasonable (although to some degree arbitrary) bound is found to be: $R_0 \lesssim 10^6\,\text{Å}$. This will serve to better direct future experiments to further test the model.

1. Introduction

Quantum Mechanics (QM) and General Relativity are the two pillars of modern physics, the former governing the microscopic world and the latter the macroscopic one, with a significant overlap. Yet, a unified description is still missing and also experimentally we are essentially ignorant about the behaviour of gravity in the quantum domain. For example we still do not know what the gravitational field generated by a spatial superposition of matter is.

The standard and by far most studied approach to unification consists in quantizing gravity [1–6]. But, in spite of many important results, a comprehensive theory of Quantum Gravity is still missing. More recently, an alternative approach is slowly emerging, aiming at modifying the structure of QM in order to accommodate gravitational effects [7–13], which predicts the existence of extra (space-time) fluctuations. This approach is also motivated by the desire of finding a solution to the well-known quantum measurement problem [14].

One of the best examples of this line of research is provided by the Diósi–Penrose (DP) model [15–19] (see [20–24] for follow ups) and belongs to a wider class of so-called collapse models [25–29]. The DP model predicts the existence of a spontaneous collapse related to gravity. As the mass of the quantum system increases and its associated gravitational field strengthens, the likelihood of spatial superposition of collapsing into well-localized states increases. As described below, the model is parametrized in terms of a length R_0, which smears the mass distribution of point particles. Equivalently, it can be seen as a high energy cutoff determining the strength of the collapse.

The different dynamics of the DP model with respect to QM allows testing it, placing experimental bounds on R_0. Specifically, these will be lower bounds, since the smaller the value of R_0, the higher the cutoff and the stronger the collapse affecting the wave function. Several experiments have been considered: matter-wave interferometry [30], neutron star heating [31], gravitational waves detector [32], heat leakage in experiments with ultralow temperature cryostats [33] and spontaneous emission of photons from bulk materials [34, 35]. Currently, the strongest bound is $R_0 \gtrsim 4 \times 10^{-10}$ m [35], which has excluded one version of the model.

While experiments keep running, it would help to constrain as much as possible the parameter space in order to better direct future tests. Here we investigate possible upper bounds, as already considered for another collapse model, the continuous spontaneous localization model [30, 36]. The theoretical bound comes from the requirement that the collapse dynamics serves its main purpose of justifying why we do not see macroscopic quantum superpositions, thus solving the quantum measurement problem. Therefore, one can claim that—to the least—it should collapse quantum superpositions of any macroscopic object before we can potentially see them. Clearly there is a lot of ambiguity in this request, given that the macroscopic domain cannot be defined precisely. We can try to remove part of this ambiguity by sharpening the request as follows: a collapse model explains classicality of the macroscopic world if a delocalized state of the smallest object which can be directly seen by the human eye collapses within its perception time. If this happens, the quantum state of any larger object will collapse even faster and classicality is secured.

Our analysis will show that the DP model, strictly speaking, does not satisfy this requirement and therefore it does not guarantee classicality. However, we will also show that the collapse becomes rapidly effective as soon as the mass of the object increases.

2. The model

The master equation describing the time evolution for the statistical operator $\hat{\rho}(t)$ of a generic N-particle system under the DP dynamics is given by

$$\frac{\mathrm{d}}{\mathrm{d}t}\hat{\rho}(t) = -\frac{i}{\hbar}\left[\hat{H}_N, \hat{\rho}(t)\right] + \mathcal{D}\left[\hat{\rho}(t)\right], \tag{1}$$

where $\hat{H}_N$ is the standard N-particle Hamiltonian and

$$\mathcal{D}\left[\hat{\rho}(t)\right] = -\frac{4\pi G}{\hbar}\int \mathrm{d}\mathbf{r}\int \mathrm{d}\mathbf{r}'\,\frac{1}{|\mathbf{r}-\mathbf{r}'|}\left[\hat{\mu}(\mathbf{r}'), \left[\hat{\mu}(\mathbf{r}), \hat{\rho}(t)\right]\right], \tag{2}$$

describes the DP non-unitary term. This term is the one responsible for the collapse, whose strength is determined by the Newtonian interaction (with G the gravitational constant) and by the mass density operator $\hat{\mu}(\mathbf{r})$ of the system. To avoid the standard divergences that occur when dealing with point-like masses, the mass density is smeared out over a width R_0, which is the only free parameter of the DP model. Specifically, by assuming for convenience that the mass density as well as the smearing are of a Gaussian form [36], for a system of N distinguishable particles of radius R_i, mass m_i and of position operator $\hat{\mathbf{x}}_i$, one has

$$\hat{\mu}(\mathbf{r}) = \sum_{i=1}^{N}\frac{m_i}{\left(2\pi R_{\mathrm{eff},i}^2\right)^{3/2}} e^{-\frac{(\mathbf{r}-\hat{\mathbf{x}}_i)^2}{2R_{\mathrm{eff},i}^2}}, \tag{3}$$

where $R_{\mathrm{eff},i} = \sqrt{R_0^2 + R_i^2}$ is the effective radius of the particle. In the limit of a point-like particle, $R_{\mathrm{eff},i}$ reduces to R_0. In the following, we will focus on the dynamics of the center-of-mass (CM) degrees of freedom alone, which can be obtained by tracing equation (1) over the relative degrees of freedom. When working with solid state materials, for values of R_0 which are not experimentally ruled out, one can safely neglect the contributions from electrons and focus on that of the nuclei because of the mass scaling of equation (3).

We assume that the system's CM is free ($\hat{H}_{\mathrm{CM}} = \frac{\hat{P}^2}{2M}$, with $M = \sum_i m_i$). In appendix A we show that for suitably short times and large superposition distances, one can neglect the Hamiltonian contribution to the dynamics ($\hat{H}_{\mathrm{CM}} \to 0$). Correspondingly, when represented in the position basis, the CM density matrix evolves according to

$$\langle \mathbf{x}|\hat{\rho}_{\mathrm{CM}}(t)|\mathbf{y}\rangle \simeq \langle \mathbf{x}|\hat{\rho}_{\mathrm{CM}}(0)|\mathbf{y}\rangle \exp\left[-t/\tau(\mathbf{x}-\mathbf{y})\right], \tag{4}$$

with $\tau(\mathbf{d}) = \hbar/\Delta E(\mathbf{d})$, where

$$\Delta E(\mathbf{d}) = -8\pi G\int \mathrm{d}\mathbf{r}\int \mathrm{d}\mathbf{r}'\,\frac{\mu(\mathbf{r})\left[\mu(\mathbf{r}'+\mathbf{d}) - \mu(\mathbf{r}')\right]}{|\mathbf{r}-\mathbf{r}'|}, \tag{5}$$

quantifies, in the Newtonian limit, the difference between the space-time curvatures generated by two well localised configurations superimposed at a distance $d = |\mathbf{d}|$. Here, $\mu(\mathbf{r})$ takes the form of equation (3) with $\hat{\mathbf{x}}_i$ replaced by the coordinate $\mathbf{x}_i$. Merging this equation with the explicit form of $\mu(\mathbf{r})$, and assuming that the N particles have the same mass m, we obtain

$$\Delta E(\mathbf{d}) = 8\pi G m^2 \sum_{i=1}^{N}\sum_{j=1}^{N} f(\mathbf{r}_{ij}, R_0, \mathbf{d}), \tag{6}$$

where

$$f(\mathbf{r}_{ij}, R_0, \mathbf{d}) = \frac{\mathrm{erf}\left(\frac{r_{ij}}{2R_{\mathrm{eff}}}\right)}{r_{ij}} - \frac{\mathrm{erf}\left(\frac{|\mathbf{d}-\mathbf{r}_{ij}|}{2R_{\mathrm{eff}}}\right)}{|\mathbf{d}-\mathbf{r}_{ij}|}, \tag{7}$$

with $\mathbf{r}_{ij} = \mathbf{x}_i - \mathbf{x}_j$ and $r_{ij} = |\mathbf{r}_{ij}|$.

3. Application

We now fix the system of interest that will be used to quantify the theoretical upper bound on R_0. We consider a plate made of a single layer of graphene [37], with a side length of $L = 25\,\mu$m corresponding to about the smallest space resolution of the eye [38]. For the sake of simplicity, one can take the system as having a square shape, corresponding to a total number of carbon atoms $N = 2 \times 10^{10}$. We assume that the CM of the system is prepared in a spatial superposition of two wavepackets of width σ at a superposition distance $d = |\mathbf{d}|$, with $\sigma \ll d$, where d has been fixed to $4L = 100\,\mu$m. This value is such that the two spatial configurations are distinguishable (namely, $d > L$ and $d > \sigma$), which is the requirement to have an actual cat state. As discussed in the Introduction, the goal is to compute the collapse time $\tau(\mathbf{d})$ of this superposition and compare it with the resolution time of the human eye, $\tau_{\mathrm{obs}} = 0.01\,$s [38].

We can quantify $\tau(\mathbf{d})$ by explicitly evaluating the sum in equation (6). Given the large value of N, which includes N^2 terms, a direct summation is not feasible. Nevertheless, since $f(\mathbf{r}_{ij}, R_0, \mathbf{d})$ depends only on the relative distance $\mathbf{r}_{ij}$, we can rewrite the double sum in equation (6) as a single weighted sum. Namely,

$$\sum_{i=1}^{N}\sum_{j=1}^{N} f(\mathbf{r}_{ij}, R_0, \mathbf{d}) = \sum_{\mathbf{r}\in\mathcal{D}} \omega(\mathbf{r}) f(\mathbf{r}, R_0, \mathbf{d}), \tag{8}$$

where $\omega(\mathbf{r})$ is the number of atoms at a distance $\mathbf{r}$ within the domain $\mathcal{D}$, which accounts for every possible distance among the atoms in the considered system. Correspondingly, the calculation strongly simplifies once considering that the atoms lie in a periodic lattice, and thus $\mathbf{r}$ becomes a function of the primitive vectors $\mathbf{a}_i$ and lattice index n_i. For a two-dimensional lattice with primitive vectors $\mathbf{a}_1$ and $\mathbf{a}_2$ and respectively N_1 and N_2 sites along these directions (where $N_1 N_2 = N$), the domain is given by

$$\mathcal{D} = \{|n_1\mathbf{a}_1 + n_2\mathbf{a}_2|, \text{where } n_i \in [-(N_i - 1), (N_i - 1)]\}, \tag{9}$$

and the weights read

$$\omega(n_1, n_2) = (N_1 - |n_1|)(N_2 - |n_2|). \tag{10}$$

Thus, the equation (8) becomes

$$\sum_{n_1=-(N_1-1)}^{N_1-1} \sum_{n_2=-(N_2-1)}^{N_2-1} \omega(n_1, n_2) f(n_1\mathbf{a}_1 + n_2\mathbf{a}_2, R_0, \mathbf{d}), \tag{11}$$

which involves the sum of $(2N_1 - 1)(2N_2 - 1) \sim 4N_1N_2 = 4N$ terms. Then, a speedup from a quadratic to a linear scaling in N is obtained, which is significant for $N \sim 10^{10}$. To be quantitative, we estimated in appendix D that the evaluation of the sum for $N = 2 \times 10^{10}$ takes around 5 min on a personal laptop by using equation (11), while it would take around 13 000 centuries by using the left-hand-side of equation (8): see appendix D, where we derive explicitly the expressions in equations (9) and (10), and extend this approach to a more general lattice. The expression in equation (11), and thus $\tau(\mathbf{d})$, is computed numerically for different values of R_0 and N, and by accounting for the actual geometry of the graphene lattice. We verified the numerical computation with analytical estimations that are derived in appendix B.

Figure 1 shows the value of $\tau(\mathbf{d})$ compared with τ_{obs}. According to the analysis, the chosen graphene plate (corresponding to the green line) collapses on a timescale that is two orders of magnitude larger than

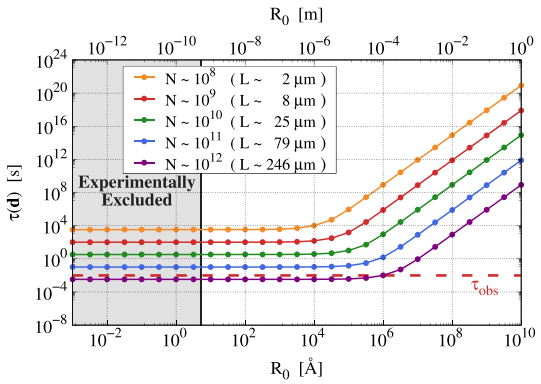

Figure 1. $\tau(\mathbf{d})$ as a function of R_0 for different sizes (equivalently, number of atoms) of a graphene square plate. The plate is assumed to be in a superposition of two localized states at a distance $|\mathbf{d}| = 4L$. The red dashed line indicates τ_{obs}. Values of R_0 for which $\tau(\mathbf{d}) > \tau_{\text{obs}}$ do not guarantee classicality. We also report the values that are currently experimentally excluded (gray shaded region) [35].

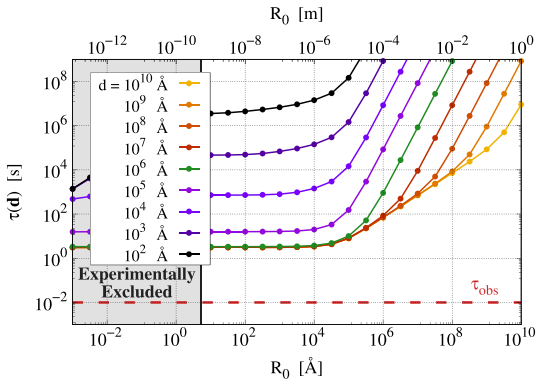

Figure 2. $\tau(\mathbf{d})$ as a function of R_0 for different values of the superposition distance d, for a graphene square plate with $N = 2 \times 10^{10}$ atoms (length $L = 25\,\mu$m). The value of $d = 4L = 10^6$ Å (green line) corresponds to that studied in figure 1(green line). The gray region is excluded experimentally.

τ_{obs}, for any value of R_0. The model does not collapse the plate fast enough with respect to the resolution time of the human eye.

The analysis also shows that, to make the collapse time shorter than τ_{obs}, one should take $\tau_{\text{obs}} \sim 3$ s, which is a too long time for requiring a macroscopic object to localize. Therefore our result is robust against changes of τ_{obs}.

A natural question is what happens if the superposition distance $d = |\mathbf{d}|$ changes. Figure 2 reports $\tau(\mathbf{d})$ for different values of d, while keeping the size of the system fixed ($L = 25\,\mu$m and $N = 2 \times 10^{10}$). With respect to the case studied in figure 1 where $d = 4L = 100\,\mu$m (red line in figure 2), we see that the collapse effect becomes stronger for larger values of d but only for values of $R_0 > L$. Conversely, for smaller values of d, the collapse effect loses strength for all values of R_0. In all cases, the collapse is not fast enough to occur before τ_{obs}. Therefore our result is robust against changes in the delocalization distance.

The next relevant question is how the collapse time $\tau(\mathbf{d})$ changes when modifying the system. We first checked what happens when increasing the size of the plate. Figure 1 shows that $\tau(\mathbf{d})$ becomes smaller than τ_{obs} when the system length L is about ten times larger than the resolution distance of the human eye ($L = 246\,\mu$m, purple line in figure 1). In this case, we obtain an upper bound on R_0 at 10^{-4} m ($= 10^6$ Å).

Next we study what happens when the system has a three dimensional structure. Specifically, we consider a cubic system made of stacked layers of graphene of length L and require again that the DP dynamics collapses it on the time-scale $\tau_{\text{obs}} = 0.01$ s. The analysis is analogous to that performed in the two-dimensional case and the results are shown in figure 3. In particular, we see that a system with $L \simeq 1.0\,\mu$m is sufficiently large to collapse within τ_{obs} for $R_0 \lesssim 10^3$ Å. We estimate that for an object of $L \simeq 10\,\mu$m, such as that considered in [39], the collapse takes place much faster (with $\tau(\mathbf{d}) \simeq 6 \times 10^{-8}$ s at the plateau) and up to a value of $R_0 \lesssim 5 \times 10^6$ Å. Such an estimation is provided by analytical calculations since the numerical approach is impractical for such a large number of atoms $N \sim 10^{14}$ (see appendix C)). We checked that the theoretical estimates match the numerical ones for smaller N. The reason why a

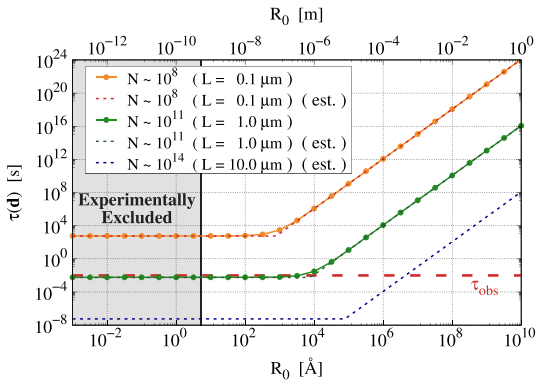

Figure 3. $\tau(\mathbf{d})$ as a function of R_0 for different number of atoms N (and thus length L) of a cubic graphene system in a superposition of two states at distance $|\mathbf{d}| = 4L$. The dashed curve provides an estimate of $\tau(\mathbf{d})$ (see SM). The gray region is excluded experimentally.

three-dimensional system collapses much more effectively compared to the case of a plate considered above is that, for the same length l, one has many more atoms involved, $\sim(L/a)^3$ vs $\sim (L/a)^2$, where a is the lattice step. Moreover, when taking the same number of atoms, the atoms are much more densely disposed in a cube than in a plate, and this makes the collapse strength grow much faster due to Newton's law in equation (2).

4. Modifications

Last, we study how robust the previous analysis is with respect to physically-motivated modifications of the model. Specifically, in the standard DP model, one assumes the noise responsible for the collapse to be white, with a Dirac-delta as the two-time correlation function. Assuming that the collapse dynamics has a physical origin, a more realistic, colored noise should be considered. The latter will be characterised by a non-trivial two-time correlation function $f(t)$. Details in the derivation of the colored collapse dynamics can be found in the literature [40–42]. Here we report the corresponding dissipator $\mathcal{D}[\hat{\rho}(t)]$ approximated to the second-order expansion in the noise, which reads

$$\mathcal{D}\left[\hat{\rho}_{\mathrm{CM}}(t)\right] = -\frac{8\pi G}{\hbar}\int_0^t \mathrm{d}s \int \mathrm{d}\mathbf{r} \int \mathrm{d}\mathbf{r}' \frac{f(t-s)}{|\mathbf{r}-\mathbf{r}'|} \times \left[\hat{\mu}(\mathbf{r}'), \left[e^{\frac{i}{\hbar}\hat{H}_N(s-t)}\hat{\mu}(\mathbf{r})\, e^{-\frac{i}{\hbar}\hat{H}_N(s-t)}, \hat{\rho}_{\mathrm{CM}}(t)\right]\right], \tag{12}$$

and substitutes that in equation (2). One recovers the standard DP model when $f(t-s) = \delta(t-s)$. Along the lines of the previous analysis, we can neglect the Hamiltonian evolution and we find that the CM density matrix evolves as in equation (4) with a time-dependent timescale $\tau(\mathbf{d}, t)$ reading

$$\tau(\mathbf{d}, t) = \frac{\hbar}{\Delta E(\mathbf{d})}\frac{t}{g(t)}, \tag{13}$$

where $g(t) = 2\int_0^t \mathrm{d}s \int_0^s \mathrm{d}s' f(s-s')$ and $\Delta E(\mathbf{d})$ as in equation (6).

An already considered choice for the two-time correlation [43, 44] is $f(t) = \Omega_{\mathrm{C}} e^{-\Omega_{\mathrm{C}}|t|}/2$, which leads to

$$g(t>0) = t\left[1 - \frac{1}{\Omega_{\mathrm{C}} t}\left(1 - e^{-\Omega_{\mathrm{C}} t}\right)\right], \tag{14}$$

where the frequency cutoff Ω_{C} becomes a further parameter of the DP model. In the limit of $\Omega_{\mathrm{C}} \to \infty$, one recovers the standard, white noise DP model, with $g(t) = t$. It is clear from equation (14) that one has $g(t) < t$ for all finite values of $\Omega_{\mathrm{C}} > 0$. Consequently, the time of collapse in the colored version of the model, given by $\tau(\mathbf{d}, t)$ in equation (13) is always larger than that of the standard DP model. Therefore, classicality takes longer to be achieved. Although one could make different choices of $f(t)$, the physically motivated ones should decay in time and we do not expect qualitative differences in the result.

5. Conclusions

The DP model finds a unique place in our efforts to understand of the quantum/gravity interplay. It proposes a new path towards the formulation of a quantum theory of gravity, by assuming that the latter is responsible

for the collapse of the wave function. The model has been and is still subject to experimental verification, with different platforms. In this work we studied how effective the DP collapse is in predicting the emergence of a macroscopic classical world from an underlying quantum structure. The conclusion is that not all macroscopic objects collapse effectively, meaning that there are some objects that do not collapse within the perception time of the human eye although they can be directly seen by it. This implies that, in principle, we should see quantum effects (whatever that means) without the need of devices, like magnifying glasses, if the macroscopic system is sufficiently well isolated. If its size increases by a couple of orders of magnitude in length or thickness, the collapse becomes fast enough.

Our analysis, therefore, shows that the quantum-to-classical transition occurs roughly at the border ($10^{10} - 10^{12}$ atoms) between what we consider meso and macro. In this region, the collapse is roughly independent from R_0 for a large range of values ($1 - 10^6$ Å). This is relevant since the existence of R_0 seems artificial, and in fact, in the past, ways to removed it were proposed [15, 18, 19], which however were not successful [34, 36]. It will be interesting to see whether this boundary set by the gravitational collapse of the wavefunction is more than a coincidence.

To fully test this boundary up to $R_0 = 10^6$ Å, experiments should be considerably developed. The most promising experiments are the so-called non-interferometric ones [29], which are based on detection of diffusive effects due to the collapse. To date, the strongest bound $R_0 \gtrsim 4$ Å is set by experiments searching for collapse-induced radiation emission from a Germanium crystal [35]. Since the predicted radiation emission rate is proportional to R_0^{-3}, an improvement of the bound on R_0 of six orders of magnitude (required to close the gap between experiments and theory) requires 18 orders of magnitude improvement on the sensitivity. While the expected radiation emission rate can be increased by considering photons at lower energies (order of few keV) [45] rather than those considered in [35], it is not obvious how to fill such a large gap. Another type of experiments which might be relevant are based on the detection of the spontaneous heating, which set a lower bound $R_0 \gtrsim 4.6 \times 10^{-2}$ Å [33]. This bound is two orders of magnitude lower than that from radiation, but it has the merit to be more robust to possible non-Markovian generalizations of the DP model. However, also in this case, the predicted increase is proportional to R_0^{-3}, requiring an improvement in sensitivity of 24 orders of magnitude to reach the upper bound.

Data availability statement

All data that support the findings of this study are included within the article (and any supplementary files).

Acknowledgments

The authors acknowledge Lajos Diósi for feedbacks on a early version of the manuscript. They acknowledge support from the University of Trieste, INFN, the PNRR MUR Projects PE0000023-NQSTI and CN00000013-HPC, the EU EIC Pathfinder Project QuCoM (10032223), the UKRI through Grant 366 No. EP/X021505/1 and FVG MICROGRANT LR2/2011 (D55-microgrants24).

Appendix A. Dynamical evolution of the center of mass of a system of N particles in the DP model

A.1. DP equation for the center of mass (CM) of the system

We start from the master equation of the DP model for N particles, which is equation (2) in the main text. Under the assumption of a rigid body, we can rewrite every position operator $\hat{\mathbf{x}}_i$ ($i = 1, \ldots, N$) of each ith particle as

$$\hat{\mathbf{x}}_i = \hat{\mathbf{x}} + \mathbf{x}_i^{(0)}, \tag{A1}$$

where $\hat{\mathbf{x}}$ is the position operator of the CM, and $\mathbf{x}_i^{(0)}$ is the classical displacement of the particle with respect to it. We substitute equation (A1) in equation (3) and merge the latter with equation (2), where for the sake of simplicity we take all $R_{\mathrm{eff},i} = R_{\mathrm{eff}}$ to be equal. This gives

$$\mathcal{D}\left[\hat{\rho}\left(t\right)\right] = -\frac{4\pi G}{\hbar}\int \mathrm{d}\mathbf{r}\int \mathrm{d}\mathbf{r}'\,\frac{1}{\left|\mathbf{r}-\mathbf{r}'\right|}\left[\hat{\mu}_{\mathrm{CM}}\left(\mathbf{r}'\right),\left[\hat{\mu}_{\mathrm{CM}}\left(\mathbf{r}\right),\hat{\rho}_{\mathrm{CM}}\right]\right], \tag{A2}$$

where $\hat{\mu}_{\rm CM}(\mathbf{r})$ is the mass density of the center of mass, which reads

$$\hat{\mu}_{\rm CM}(\mathbf{r}) = \sum_{i=1}^{N} \frac{m_i}{\left(2\pi R_{\rm eff}^2\right)^{3/2}} \exp\left[-\frac{\left(\hat{\mathbf{x}} + \mathbf{x}_i^{(0)} - \mathbf{r}\right)^2}{2R_{\rm eff}^2}\right]. \tag{A3}$$

Then, by tracing over the internal degrees of freedom, and expressing the CM mass density in Fourier space

$$\hat{\mu}_{\rm CM}(\mathbf{r}) = \sum_{i=1}^{N} \frac{m_i}{(2\pi)^3} \int \mathrm{d}\mathbf{q}\, e^{-i\mathbf{q}\cdot\left(\hat{\mathbf{x}}+\mathbf{x}_i^{(0)}-\mathbf{r}\right)} e^{-R_{\rm eff}^2 q^2/2}, \tag{A4}$$

we find the master equation for the center of mass: $\frac{\mathrm{d}}{\mathrm{d}t}\hat{\rho}_{\rm CM}(t) = -\frac{i}{\hbar}\left[\hat{H}_{\rm CM}, \hat{\rho}_{\rm CM}(t)\right] + \mathcal{D}[\hat{\rho}_{\rm CM}(t)]$, where

$$\begin{aligned}&\mathcal{D}\left[\hat{\rho}_{\rm CM}(t)\right]\\ &= -\frac{4\pi G}{\hbar}\int \mathrm{d}\mathbf{r}\int \mathrm{d}\mathbf{r}'\frac{1}{|\mathbf{r}-\mathbf{r}'|}\sum_{i,j=1}^{N}\frac{m_i m_j}{(2\pi)^6}\int \mathrm{d}\mathbf{q}\int \mathrm{d}\mathbf{k}\, e^{-R_{\rm eff}^2\left(\mathbf{q}^2+\mathbf{k}^2\right)/2} e^{-i\mathbf{q}\cdot\left(\mathbf{x}_i^{(0)}-\mathbf{r}'\right)} e^{-i\mathbf{k}\cdot\left(\mathbf{x}_j^{(0)}-\mathbf{r}\right)}\left[e^{-i\mathbf{q}\cdot\hat{\mathbf{x}}}, \left[e^{-i\mathbf{k}\cdot\hat{\mathbf{x}}}, \hat{\rho}(t)\right]\right].\end{aligned} \tag{A5}$$

We can simplify such an expression through the use of the following identity

$$\frac{1}{|\mathbf{r}-\mathbf{r}'|} = \frac{1}{2\pi^2}\int \mathrm{d}\mathbf{p}\,\frac{e^{-i\mathbf{p}\cdot\left(\mathbf{r}-\mathbf{r}'\right)}}{p^2}, \tag{A6}$$

and straightforward calculations lead to the following dynamical evolution of the CM of the system

$$\frac{\mathrm{d}\hat{\rho}_{\rm CM}(t)}{\mathrm{d}t} = -\frac{i}{\hbar}\left[\hat{H}_{\rm CM}, \hat{\rho}_{\rm CM}(t)\right] + \int \mathrm{d}\mathbf{p}\, F(\mathbf{p})\left(e^{i\mathbf{p}\cdot\hat{\mathbf{x}}}\hat{\rho}_{\rm CM}(t)\, e^{-i\mathbf{p}\cdot\hat{\mathbf{x}}} - \hat{\rho}_{\rm CM}(t)\right), \tag{A7}$$

where we introduced

$$F(\mathbf{p}) = \frac{4G}{\pi\hbar}\sum_{i,j=1}^{N} m_i m_j \frac{e^{-R_{\rm eff}^2 p^2}}{p^2} e^{i\mathbf{p}\cdot\left(\mathbf{x}_i^{(0)}-\mathbf{x}_j^{(0)}\right)}, \tag{A8}$$

which is the form factor accounting for the dimension and form of the system. Equation (A7) is the master equation of the DP model for the CM of a N-particle system.

A.2. Analytic solution of the equation for the center of mass

To solve the master equation for the CM, it is convenient to introduce the characteristic function χ [46, 47], which is defined as

$$\chi(\boldsymbol{\nu}, \boldsymbol{\mu}, t) = \mathrm{Tr}\left[\hat{\rho}_{\rm CM}(t)\, e^{-\frac{i}{\hbar}\left(\boldsymbol{\nu}\cdot\hat{\mathbf{x}}+\boldsymbol{\mu}\cdot\hat{\mathbf{p}}\right)}\right]. \tag{A9}$$

For the sake of simplicity, we assume that the CM is free, i.e. $\hat{H}_{\rm CM} = \hat{\mathbf{p}}^2/2M$. Thus, given the master equation (A7) for a free particle, one finds that the characteristic function satisfies the following equation [47]

$$\frac{\mathrm{d}}{\mathrm{d}t}\chi(\boldsymbol{\nu}, \boldsymbol{\mu}, t) = \frac{1}{M}\boldsymbol{\nu}\cdot\nabla_{\boldsymbol{\mu}}\chi(\boldsymbol{\nu}, \boldsymbol{\mu}, t) + \frac{1}{\hbar}\left(E(\boldsymbol{\mu}) - E(\mathbf{0})\right)\chi(\boldsymbol{\nu}, \boldsymbol{\mu}, t), \tag{A10}$$

where

$$E(\boldsymbol{\mu}) = \hbar\int \mathrm{d}\mathbf{p}\, F(\mathbf{p})\, e^{i\boldsymbol{\mu}\cdot\mathbf{p}}, \tag{A11}$$

The solution to equation (A10) is given by [47]

$$\chi(\boldsymbol{\nu}, \boldsymbol{\mu}, t) = \chi_0\left(\boldsymbol{\nu}, \boldsymbol{\mu} + \boldsymbol{\nu}\tfrac{t}{M}, t\right)\exp\left[\tfrac{1}{\hbar}\int_0^t \mathrm{d}\tau\left(E\left(\boldsymbol{\mu} + \boldsymbol{\nu}\tfrac{\tau}{M}\right) - E(\mathbf{0})\right)\right], \tag{A12}$$

where $\chi_0(\boldsymbol{\nu}, \boldsymbol{\mu}, t)$ satisfies

$$\frac{\mathrm{d}}{\mathrm{d}t}\chi_0(\boldsymbol{\nu}, \boldsymbol{\mu}, t) = \frac{1}{M}\boldsymbol{\nu}\cdot\nabla_{\boldsymbol{\mu}}\chi_0(\boldsymbol{\nu}, \boldsymbol{\mu}, t), \tag{A13}$$

and corresponds to the characteristic function for the Hamiltonian dynamics. This corresponds to the standard quantum mechanical predictions.

To reconstruct the matrix elements of $\hat{\rho}_{\rm CM}(t)$, one employs [47]

$$\langle \mathbf{x}|\hat{\rho}_{\rm CM}(t)|\mathbf{y}\rangle = \frac{1}{(2\pi\hbar)^3}\int \mathrm{d}\boldsymbol{\nu}\, e^{-\frac{i}{2\hbar}\boldsymbol{\nu}\cdot(\mathbf{x}+\mathbf{y})}\chi(\boldsymbol{\nu},\mathbf{x}-\mathbf{y},t). \tag{A14}$$

We can express $\langle \mathbf{x}|\hat{\rho}_{\rm CM}(t)|\mathbf{y}\rangle$ in terms of the matrix elements of $\hat{\rho}^{\rm QM}_{\rm CM}(t)$, which is the statistical operator corresponding to the quantum dynamical evolution (that related to χ_0 alone). Such a relation reads

$$\langle \mathbf{x}|\hat{\rho}_{\rm CM}(t)|\mathbf{y}\rangle = \frac{1}{(2\pi\hbar)^3}\int \mathrm{d}\boldsymbol{\nu}\int \mathrm{d}\mathbf{z}\, e^{\frac{i}{\hbar}\boldsymbol{\nu}\cdot\mathbf{z}}\langle \mathbf{z}+\mathbf{x}|\hat{\rho}^{\rm QM}_{\rm CM}(t)|\mathbf{z}+\mathbf{y}\rangle \exp\left[\frac{1}{\hbar}\int_0^t \mathrm{d}\tau\left(E\left(\boldsymbol{\nu}\frac{\tau}{M}+\mathbf{x}-\mathbf{y}\right)-E(\mathbf{0})\right)\right], \tag{A15}$$

with $E(\mathbf{x})$ being defined as in equation (A11) and which takes the explicit form of

$$E(\boldsymbol{\mu}) = 8\pi G\sum_{i,j=1}^{N} m_i m_j \frac{\mathrm{erf}\left(\frac{|\mathbf{x}_i^{(0)}-\mathbf{x}_j^{(0)}+\boldsymbol{\mu}|}{2R_{\rm eff}}\right)}{|\mathbf{x}_i^{(0)}-\mathbf{x}_j^{(0)}+\boldsymbol{\mu}|}, \tag{A16}$$

for the DP model. Finally, the expression in equation (6), namely

$$\Delta E(\mathbf{d}) = 8\pi G m^2\sum_{i,j=1}^{N}\left[\frac{\mathrm{erf}\left(\frac{r_{ij}}{2R_{\rm eff}}\right)}{r_{ij}}-\frac{\mathrm{erf}\left(\frac{|\mathbf{d}+\mathbf{r}_{ij}|}{2R_{\rm eff}}\right)}{|\mathbf{d}+\mathbf{r}_{ij}|}\right], \tag{A17}$$

is obtained with $\Delta E(\mathbf{d}) = E(\mathbf{d}) - E(\mathbf{0})$.

A.3. Neglecting the free evolution $\hat{H}_{\rm CM}$ in the DP master equation

In the following, we investigate the conditions under which one can safely neglect the free evolution (i.e. $\hat{H}_{\rm CM}$) when quantifying the collapse action of the DP model on the CM. Specifically, we focus on the matrix element of equation (A15) for the case of an initial state $\psi(\mathbf{x},0)$ being in a superposition of two equal Gaussians centered in $\pm\mathbf{d}/2$. Hence, we have

$$\psi(\mathbf{x},0) = \frac{1}{\mathcal{N}}\left[e^{-\frac{1}{2\sigma^2}(\mathbf{x}-\mathbf{d}/2)^2}+e^{-\frac{1}{2\sigma^2}(\mathbf{x}+\mathbf{d}/2)^2}\right], \tag{A18}$$

where

$$\mathcal{N} = \left[2\left(\sqrt{\pi}\sigma\right)^3\left(1+e^{-\frac{d^2}{4\sigma^2}}\right)\right]^{1/2}, \tag{A19}$$

is the corresponding normalization constant, $d = |\mathbf{d}|$, and σ is the Gaussian spread. The free, quantum mechanical evolution of the CM, where $\hat{H}_{\rm CM} = \hat{\mathbf{p}}^2/2M$, leads to the following expression for the state at a time t

$$\psi(\mathbf{x},t) = \frac{1}{\mathcal{N}}\left(\frac{\sigma}{\sqrt{\sigma^2+\frac{i\hbar t}{M}}}\right)^3\left(e^{-\frac{(x+d/2)^2}{2\left(\sigma^2+\frac{i\hbar t}{M}\right)}}+e^{-\frac{(x-d/2)^2}{2\left(\sigma^2+\frac{i\hbar t}{M}\right)}}\right). \tag{A20}$$

We now focus on the matrix element $\langle -\mathbf{d}/2|\hat{\rho}_{\rm CM}(t)|\mathbf{d}/2\rangle$, which measures the coherence between the two wave packets. Due to the spatial decoherence induced by the DP model, we expect this term to decay. Our goal is to understand under which conditions, when computing this term, $\hat{H}_{\rm CM}$ can be neglected.

From equation (A20), we can directly calculate the matrix element for the density operator in the standard quantum mechanical case as

$$\langle \mathbf{x}|\hat{\rho}^{\rm QM}_{\rm CM}(t)|\mathbf{y}\rangle = \psi^*(\mathbf{x},t)\,\psi(\mathbf{y},t) = \frac{1}{\mathcal{N}^2}\frac{\sigma^6\left(e^{-\frac{(x+d/2)^2}{2\left(\sigma^2-\frac{i\hbar t}{M}\right)}}+e^{-\frac{(x-d/2)^2}{2\left(\sigma^2-\frac{i\hbar t}{M}\right)}}\right)\left(e^{-\frac{(y+d/2)^2}{2\left(\sigma^2+\frac{i\hbar t}{M}\right)}}+e^{-\frac{(y-d/2)^2}{2\left(\sigma^2+\frac{i\hbar t}{M}\right)}}\right)}{\left(\sigma^4+\left(\frac{\hbar t}{M}\right)^2\right)^{3/2}}, \tag{A21}$$

which can be then inserted in equation (A15). After integrating over $\mathbf{z}$, we obtain

$$\langle -\mathbf{d}/2|\hat{\rho}_{\rm CM}(t)|\mathbf{d}/2\rangle = \mathcal{K}_1+\mathcal{K}_2+\mathcal{K}_3, \qquad \text{where} \qquad \mathcal{K}_j = \int \mathrm{d}\boldsymbol{\nu}\, e^{-\boldsymbol{\nu}^2}\mathcal{F}(\mathbf{d}/2,\boldsymbol{\nu})\,\mathcal{G}_j(\mathbf{d}/2,\boldsymbol{\nu}). \tag{A22}$$

where we defined

$$\begin{aligned}
&\mathcal{G}_1(\mathbf{d}/2,\boldsymbol{\nu}) = 1,\\
&\mathcal{G}_2(\mathbf{d}/2,\boldsymbol{\nu}) = \exp\left(-\frac{d^2}{\sigma^2}\right)\exp\left(-\frac{2\hbar t}{M\sigma^2}\frac{\boldsymbol{\nu}\cdot\mathbf{d}}{\sqrt{1+\left(\frac{\hbar t}{M\sigma^2}\right)^2}}\right),\\
&\mathcal{G}_3(\mathbf{d}/2,\boldsymbol{\nu}) = \exp\left(-\frac{d^2}{4\sigma^2}\right)\exp\left(-\frac{\hbar t}{M\sigma^2}\frac{\boldsymbol{\nu}\cdot\mathbf{d}}{\sqrt{1+\left(\frac{\hbar t}{M\sigma^2}\right)^2}}\right)\times 2\cos\left(\frac{1}{\sigma}\frac{\boldsymbol{\nu}\cdot\mathbf{d}}{\sqrt{1+\left(\frac{\hbar t}{M\sigma^2}\right)^2}}\right),\\
&\mathcal{F}(\mathbf{d}/2,\boldsymbol{\nu}) = \frac{1}{\pi^{3/2}\mathcal{N}^2\left[1+\left(\frac{\hbar t}{M\sigma^2}\right)^2\right]^{3/2}}\exp\left[\int_0^t \mathrm{d}\tau\left(f\left(\mathbf{d}+2\sigma\frac{\tau}{t}\frac{\boldsymbol{\nu}}{\sqrt{1+\left(\frac{M\sigma^2}{\hbar t}\right)^2}}\right)-f(\mathbf{0})\right)\right].
\end{aligned} \tag{A23}$$

We notice that, the exponential factor in equation (A22) limits the main contributions to $\mathcal{K}_j$ to the vectors $\boldsymbol{\nu}$ such that $|\boldsymbol{\nu}|\leqslant 1$. Moreover, for $d\gg\sigma$, we can approximate the argument in the exponential of $\mathcal{F}(\mathbf{d}/2,\boldsymbol{\nu})$ in equation (A23) as $(f(\mathbf{d})-f(\mathbf{0}))t$, which is possible since $\boldsymbol{\nu}$ is limited. These two approximations allow to easily compute $\mathcal{K}_j$, which read

$$\begin{aligned}
\mathcal{K}_1 &= \frac{1}{\mathcal{N}^2}\left(\frac{1}{1+\left(\frac{\hbar t}{M\sigma^2}\right)^2}\right)^{3/2}\exp\left[\left(f(\mathbf{d})-f(\mathbf{0})\right)t\right],\\
\mathcal{K}_2 &= \exp\left[-\frac{d^2}{\sigma^2}\left(1-\frac{t^2\hbar^2}{M^2\sigma^4+t^2\hbar^2}\right)\right]\mathcal{K}_1,\\
\mathcal{K}_3 &= 2\exp\left(-\frac{d^2}{4\sigma^2}\frac{2M^2\sigma^4}{M^2\sigma^4+t^2\hbar^2}\right)\cos\left(\frac{M\sigma^2 t\hbar}{M^2\sigma^4+t^2\hbar^2}\frac{d^2}{2\sigma^2}\right)\mathcal{K}_1.
\end{aligned} \tag{A24}$$

For small times, satisfying $t\ll M\sigma^2/\hbar$, we see that the expressions for $\mathcal{K}_i$ reduce to

$$\begin{aligned}
\mathcal{K}_1 &= \frac{1}{\mathcal{N}^2}\exp\left[f(\mathbf{d})-f(\mathbf{0})\right)t],\\
\mathcal{K}_2 &= e^{-\frac{d^2}{\sigma^2}}\mathcal{K}_1,\\
\mathcal{K}_3 &= 2e^{-\frac{d^2}{2\sigma^2}}\mathcal{K}_1,
\end{aligned} \tag{A25}$$

and therefore

$$\langle -\mathbf{d}/2|\hat{\rho}_{\rm CM}(t)|\mathbf{d}/2\rangle = \frac{1}{\mathcal{N}^2}\left(1+e^{-\frac{d^2}{2\sigma^2}}\right)^2\exp\left[\left(f(\mathbf{d})-f(\mathbf{0})\right)t\right], \tag{A26}$$

which is the expression that one would obtain if the evolution due to the Hamiltonian $\hat{H}_{\rm CM}$ is neglected. Indeed, when neglecting $\hat{H}_{\rm CM}$, one has that equation (A10) changes in

$$\frac{\mathrm{d}}{\mathrm{d}t}\chi(\boldsymbol{\nu},\boldsymbol{\mu},t) = \left(f(\boldsymbol{\mu})-f(\mathbf{0})\right)\chi(\boldsymbol{\nu},\boldsymbol{\mu},t), \tag{A27}$$

whose trivial solution is

$$\chi(\boldsymbol{\nu},\boldsymbol{\mu},t) = \chi(\boldsymbol{\nu},\boldsymbol{\mu},0)\exp\left[\left(f(\mathbf{d})-f(\mathbf{0})\right)t\right], \tag{A28}$$

where $\chi(\boldsymbol{\nu},\boldsymbol{\mu},0)$ can be obtained from equation (A9) by setting $t=0$. Correspondingly, equation (A15) changes in

$$\langle\mathbf{x}|\hat{\rho}_{\rm CM}(t)|\mathbf{y}\rangle = \langle\mathbf{x}|\hat{\rho}^{\rm QM}_{\rm CM}(0)|\mathbf{y}\rangle\exp\left[\left(f(\mathbf{d})-f(\mathbf{0})\right)t\right], \tag{A29}$$

where

$$\langle\mathbf{x}|\hat{\rho}^{\rm QM}_{\rm CM}(0)|\mathbf{y}\rangle = \psi^*(\mathbf{x},0)\,\psi(\mathbf{y},0). \tag{A30}$$

The trivial substitution of the latter expression in equation (A29), and setting $\mathbf{x} = -\mathbf{d}/2$ and $\mathbf{y} = \mathbf{d}/2$ leads to equation (A26). Thus, under these assumptions, we can safely neglect the evolution due to $\hat{H}_{\mathrm{CM}}$ in the DP model.

Appendix B. Analytical study of the behaviour of $\Delta E(\mathbf{d})$

We study the behaviour of $\Delta E(\mathbf{d})$ for a crystal of N atoms of mass m. We study a two-dimensional crystal with a monoatomic square lattice with the same lattice step a, and with crystal's sides of approximately the same length L. Accordingly $L \sim \sqrt{N}a$. One can trivially generalize to the case of different length sides. Specifically, we analyze the case of a spatial superposition of the form in equation (A18), where the two branches of the superposition are well separated with respect to L. Hence, the length hierarchy is given by $a \ll L \ll d$. With this setting, the vectors $\mathbf{r}_{ij}$ can only take discrete values, namely $\mathbf{r}_{ij} = a(n_x^i - n_x^j, n_y^i - n_y^j)$, where $n_k^i \in \mathbb{Z}$.

In the following, we analyze analytically the behaviour of $\Delta E(\mathbf{d})$ in equation (A17) for different values of R_{eff}. Specifically, we provide the contributions to the sum from the first and second term in the square bracket. Namely, these are

$$\begin{aligned} S_1 &= \sum_{i,j=1}^{N} \frac{\mathrm{erf}\left(\frac{r_{ij}}{2R_{\mathrm{eff}}}\right)}{r_{ij}}, \\ S_2 &= \sum_{i,j=1}^{N} \frac{\mathrm{erf}\left(\frac{|\mathbf{d}+\mathbf{r}_{ij}|}{2R_{\mathrm{eff}}}\right)}{|\mathbf{d}+\mathbf{r}_{ij}|}, \end{aligned} \tag{B1}$$

so that $\Delta E(\mathbf{d}) = 8\pi G m^2 (S_1 - S_2)$. The analytical expressions will be then compared with those obtained numerically in figure 4.

B.1. Analytical estimation of the first contribution to the sum S_1

The first contribution to the sum S_1 is analysed in four different intervals of interest: $R_{\mathrm{eff}} \leqslant a$, $a \leqslant R_{\mathrm{eff}} \leqslant L$, $L \leqslant R_{\mathrm{eff}} \leqslant d$ and $d \leqslant R_{\mathrm{eff}}$. We split the sum in S_1 in two contributions: the sum of the terms with $i = j$ and the sum where $i \neq j$.

When $i = j$, we have $r_{ii} = 0$ and thus the corresponding sum reads

$$\sum_{i=1}^{N} \frac{\mathrm{erf}\left(\frac{r_{ii}}{2R_{\mathrm{eff}}}\right)}{r_{ii}} \underset{r_{ii}\to 0}{\longrightarrow} \sum_{i=1}^{N} \frac{1}{\sqrt{\pi} R_{\mathrm{eff}}}, \tag{B2}$$

and we have

$$S_1 = \frac{N}{\sqrt{\pi} R_{\mathrm{eff}}} + \sum_{\substack{i,j=1 \\ i\neq j}}^{N} \frac{\mathrm{erf}\left(\frac{r_{ij}}{2R_{\mathrm{eff}}}\right)}{r_{ij}}, \tag{B3}$$

which we will study below.

B.1.1. First interval: $R_{eff} \leqslant a$

Consider the case $R_{\mathrm{eff}} \leqslant a$. For all terms with $i \neq j$, we have that $r_{ij} \geqslant a$. Indeed, the minimal value of $r_{ij} = a$ is attained for the first nearest neighbor atoms. This implies $R_{\mathrm{eff}} \leqslant r_{ij}$. In particular, we can divide the contributions to the sum in two cases

$$\begin{cases} \text{for } 1 \leqslant \frac{r_{ij}}{R_{\mathrm{eff}}} \leqslant 4, & \frac{1}{2} < \mathrm{erf}\left(\frac{r_{ij}}{2R_{\mathrm{eff}}}\right) < 1, \\ \text{for } 4 \leqslant \frac{r_{ij}}{R_{\mathrm{eff}}}, & \mathrm{erf}\left(\frac{r_{ij}}{2R_{\mathrm{eff}}}\right) \sim 1. \end{cases} \tag{B4}$$

We can then employ these to set an upper and lower bound on the sum by approximating that all the terms weight the same independently of the value of r_{ij}. We have then

$$\sum_{\substack{i,j=1 \\ i\neq j}}^{N} \frac{1}{2}\frac{1}{r_{ij}} \leqslant \sum_{\substack{i,j=1 \\ i\neq j}}^{N} \frac{\mathrm{erf}\left(\frac{r_{ij}}{2R_{\mathrm{eff}}}\right)}{r_{ij}} \leqslant \sum_{\substack{i,j=1 \\ i\neq j}}^{N} \frac{1}{r_{ij}}. \tag{B5}$$

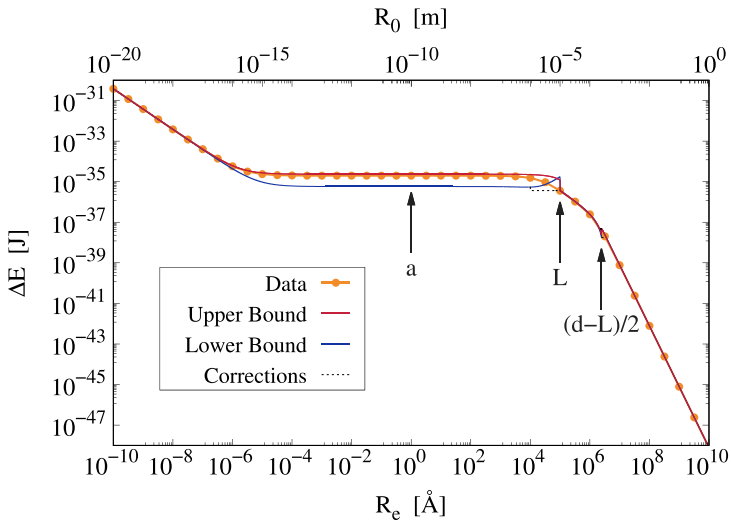

Figure 4. Analytical upper (red line) and lower (blue line) bounds for ΔE as a function of R_{eff}. The dashed black line provides a better estimation of the lower bound for values of $R_{\text{eff}} \simeq L$ and $(d-L)/2$ by exploiting the monotonicity of $\Delta E(\mathbf{d})$. For comparison, we reported the exact values computed numerically (orange dots). The vertical arrows correspond to the values of R_{eff} equal to a, L and $(d-L)/2$ (from left to right). The values of the parameters are: $a = 1.0$ Å, $N = 10^{10}$, $L = 10^5$ Å and $d = 50L = 5 \times 10^6$ Å.

Then, both limits depend on the same sum, which can be rewritten as

$$\sum_{\substack{i,j=1\\ i\neq j}}^{N} \frac{1}{r_{ij}} = \sum_{\substack{i,j=1\\ i\neq j}}^{N} \frac{1}{a\sqrt{\left(n_x^i - n_x^j\right)^2 + \left(n_y^i - n_y^j\right)^2}}, \tag{B6}$$

where $n_k^i \in [-\sqrt{N}/2, \sqrt{N}/2]$. We first fix the ith particle as that at the center of the lattice with $n_x^i = n_y^i = 0$ and sum over j. This term provides an upper bound on the other contributions of the i-sum, since fixing the ith atom to any other in the lattice would provide a smaller contribution. Then, the corresponding vector $\mathbf{r}_{ij} = a(-n_x^j, -n_y^j)$ has a length of $r_{ij} = a\sqrt{(n_x^j)^2 + (n_y^j)^2}$. We obtain

$$\sum_{\substack{i,j=1\\ i\neq j}}^{N} \frac{1}{r_{ij}} \leqslant \sum_{i=1}^{N} \sum_{\substack{n_x^j, n_y^j = -\sqrt{N}/2\\ (n_x^j, n_y^j)\neq(0,0)}}^{\sqrt{N}/2} \frac{1}{a\sqrt{\left(n_x^j\right)^2 + \left(n_y^j\right)^2}} = \frac{N}{a} \sum_{\substack{n_x^j, n_y^j = -\sqrt{N}/2\\ (n_x^j, n_y^j)\neq(0,0)}}^{\sqrt{N}/2} \frac{1}{\sqrt{\left(n_x^j\right)^2 + \left(n_y^j\right)^2}}. \tag{B7}$$

The contribution in right hand side of equation (B7) can be approximated with the following integral

$$\frac{N}{a} \int_{-\sqrt{N}/2}^{\sqrt{N}/2} \mathrm{d}x \int_{-\sqrt{N}/2}^{\sqrt{N}/2} \mathrm{d}y \, \frac{1}{\sqrt{x^2+y^2}} = \frac{\eta_+ N\sqrt{N}}{a}, \tag{B8}$$

where $\eta_+ = 2\ln(3+2\sqrt{2}) \simeq 3.5$.

Similarly, if we fix the ith atom to the corner of the lattice, we provide a lower bound. The corresponding vector $\mathbf{r}_{ij} = a(-\sqrt{N}/2 - n_x^j, -\sqrt{N}/2 - n_y^j)$ has a length of $r_{ij} = a\sqrt{(\sqrt{N}/2 + n_x^j)^2 + (\sqrt{N}/2 + n_y^j)^2}$. Thus, we have

$$\sum_{\substack{i,j=1\\ i\neq j}}^{N} \frac{1}{r_{ij}} \geqslant \sum_{i=1}^{N} \sum_{\substack{n_x^j, n_y^j = -\sqrt{N}/2\\ (n_x^j, n_y^j)\neq(0,0)}}^{\sqrt{N}/2} \frac{1}{a\sqrt{\left(\sqrt{N}/2 + n_x^j\right)^2 + \left(\sqrt{N}/2 + n_y^j\right)^2}}. \tag{B9}$$

Similarly as done before, we can approximate the sum to an integral, which reads

$$\frac{N}{a} \int_{-\sqrt{N}/2}^{\sqrt{N}/2} \mathrm{d}x \int_{-\sqrt{N}/2}^{\sqrt{N}/2} \mathrm{d}y \, \frac{1}{\sqrt{\left(\sqrt{N}/2 + x\right)^2 + \left(\sqrt{N}/2 + y\right)^2}} = \frac{2\eta_- N\sqrt{N}}{a}, \tag{B10}$$

where $\eta_- = \mathrm{arcsinh}(1) \simeq 0.9$. By merging the inequality in equation (B5) with those in equations (B7) and (B9), we find the bounds on equation (B3) being

$$\frac{N}{\sqrt{\pi}R_{\mathrm{eff}}} + \frac{\eta_- N\sqrt{N}}{a} \leqslant S_1 \leqslant \frac{N}{\sqrt{\pi}R_{\mathrm{eff}}} + \frac{\eta_+ N\sqrt{N}}{a}. \tag{B11}$$

Specifically, for

$$R_{\mathrm{eff}} \lesssim \frac{a}{\eta_\pm\sqrt{\pi N}}, \tag{B12}$$

the first contribution is stronger and corresponds to a behaviour going as $\sim R_{\mathrm{eff}}^{-1}$. Conversely, for larger values of R_{eff} (but still within the first interval, $R_{\mathrm{eff}} < a$), the first term in equation (B11) is negligible with respect to the second one, which is independent from R_{eff}.

B.1.2. Second interval: $a \leqslant R_{eff} \leqslant L$

In the second interval, $a \leqslant R_{\mathrm{eff}} \leqslant L$, we have that r_{ij} can be comparable with R_{eff}. Namely, for $i \neq j$, we have $a \leqslant r_{ij} \leqslant \sqrt{2}L$. Due to the comparable interval of r_{ij} and R_{eff}, we have several edge effects that make the analytical estimation more difficult. Since one can approximate fairly enough the error function to

$$\mathrm{erf}\left(\frac{x}{2}\right) \simeq \begin{cases} \frac{x}{\sqrt{\pi}}, & x \leqslant 2, \\ 1, & x \geqslant 2, \end{cases} \tag{B13}$$

we divide the sum in terms for which $r_{ij} \leqslant 2R_{\mathrm{eff}}$ and terms for which $r_{ij} \geqslant 2R_{\mathrm{eff}}$.

For $r_{ij} \leqslant 2R_{\mathrm{eff}}$,

$$\frac{\mathrm{erf}\left(\frac{r_{ij}}{2R_{\mathrm{eff}}}\right)}{r_{ij}} \simeq \frac{1}{\sqrt{\pi}R_{\mathrm{eff}}}, \tag{B14}$$

and, given the ith atom, there are roughly $(2R_{\mathrm{eff}}/a)^2$ atoms j that are at most at a distance $2R_{\mathrm{eff}}$. Thus, the contribution to the second term in equation (B3) for $r_{ij} \leqslant 2R_{\mathrm{eff}}$ can be evaluated to

$$\sum_{\substack{i,j=1 \\ i\neq j,\, r_{ij}\leqslant 2R_{\mathrm{eff}}}}^{N} \frac{\mathrm{erf}\left(\frac{r_{ij}}{2R_{\mathrm{eff}}}\right)}{r_{ij}} \simeq N \times \left(\frac{2R_{\mathrm{eff}}}{a}\right)^2 \frac{1}{\sqrt{\pi}R_{\mathrm{eff}}} = 4N\frac{R_{\mathrm{eff}}}{\sqrt{\pi}a^2}. \tag{B15}$$

For $r_{ij} \geqslant 2R_{\mathrm{eff}}$,

$$\frac{\mathrm{erf}\left(\frac{r_{ij}}{2R_{\mathrm{eff}}}\right)}{r_{ij}} \simeq \frac{1}{r_{ij}}. \tag{B16}$$

Then, the corresponding contribution to the sum can be rewritten as

$$\sum_{\substack{i,j=1 \\ i\neq j,\, r_{ij}\geqslant 2R_{\mathrm{eff}}}}^{N} \frac{\mathrm{erf}\left(\frac{r_{ij}}{2R_{\mathrm{eff}}}\right)}{r_{ij}} \simeq \sum_{\substack{i,j=1 \\ i\neq j}}^{N} \frac{1}{r_{ij}} - \sum_{\substack{i,j=1 \\ i\neq j,\, r_{ij}\leqslant 2R_{\mathrm{eff}}}}^{N} \frac{1}{r_{ij}}, \tag{B17}$$

where the upper and lower bounds to the first sum are respectively given by equations (B7) and (B9). Also the second term can be bounded. A lower bound is given by setting all the r_{ij} to the maximum distance being $2R_{\mathrm{eff}}$, namely

$$\sum_{\substack{i,j=1 \\ i\neq j,\, r_{ij}\leqslant 2R_{\mathrm{eff}}}}^{N} \frac{1}{r_{ij}} \geqslant \sum_{\substack{i,j=1 \\ i\neq j,\, r_{ij}\leqslant 2R_{\mathrm{eff}}}}^{N} \frac{1}{2R_{\mathrm{eff}}} = N \times \left(\frac{2R_{\mathrm{eff}}}{a}\right)^2 \frac{1}{2R_{\mathrm{eff}}} = \frac{4NR_{\mathrm{eff}}}{a^2}. \tag{B18}$$

An upper bound is instead obtained by fixing the ith atom to the center of the lattice, and approximating the sum over j to an integral in spherical coordinates. Namely,

$$\sum_{\substack{i,j=1 \\ i\neq j,\, r_{ij}\leqslant 2R_{\mathrm{eff}}}}^{N} \frac{1}{r_{ij}} \leqslant \frac{2\pi N}{a}\mathcal{F}_G \int_1^{\frac{2R_{\mathrm{eff}}}{a}} \mathrm{d}r = \frac{2\pi N}{a}\mathcal{F}_G\left(\frac{2R_{\mathrm{eff}}}{a} - 1\right), \tag{B19}$$

where $\mathcal{F}_G$ is a geometrical factor accounting for couples of atoms (i,j) that are counted in the sum but do not appertain to the lattice (indeed, one can have that $2R_{\rm eff} = 2L \geqslant \sqrt{2}L$ being the maximum distance r_{ij}), and accounts for the ratio of the area of a square lattice of length $2R_{\rm eff}$ with the spam of the considered r_{ij}, namely that of a planar toric lattice of internal radius a and external radius $2R_{\rm eff}$:

$$\mathcal{F}_G = \frac{L^2}{L^2 + 4LR_{\rm eff} + \pi R_{\rm eff}^2} \frac{4R_{\rm eff}^2}{\pi\left(4R_{\rm eff}^2 - a^2\right)}. \tag{B20}$$

By summing the contributions from equations (B15) and (B17), we find that equation (B3) is bounded as follows

$$\frac{N}{\sqrt{\pi}R_{\rm eff}} + \frac{\eta_- N\sqrt{N}}{a} + \frac{4NR_{\rm eff}}{\sqrt{\pi}a^2} - \frac{2\pi N}{a}\mathcal{F}_G\left(\frac{2R_{\rm eff}}{a} - 1\right) \leqslant S_1 \leqslant \frac{N}{\sqrt{\pi}R_{\rm eff}} + \frac{\eta_+ N\sqrt{N}}{a} + \frac{4NR_{\rm eff}}{a^2}\left(\frac{1}{\sqrt{\pi}} - 1\right). \tag{B21}$$

Specifically, for small values of $R_{\rm eff} \gtrsim a$ the main contribution comes from the second term, i.e. $\eta_\pm N\sqrt{N}/a$, being independent from $R_{\rm eff}$. For large values of $R_{\rm eff} \lesssim L$, the third and fourth terms become the dominant ones. In particular, a change in the $R_{\rm eff}$ dependence of S_1 appears from values of

$$R_{\rm eff} \gtrsim \frac{\eta_\pm N\sqrt{N\pi}a}{4}. \tag{B22}$$

B.1.3. Third interval: $L \leqslant R_{eff} \leqslant d$

In this regime $r_{ij} \leqslant R_{\rm eff}$ for $r_{ij} \leqslant L$. However, one also has distances such that $L \leqslant r_{ij} \leqslant \sqrt{2}L$ for which one can have $r_{ij} \geqslant R_{\rm eff}$. Nevertheless, we have that $\sqrt{2}L < 2L \leqslant 2R_{\rm eff}$, which implies that $r_{ij} \leqslant \sqrt{2}L < 2R_{\rm eff}$. Consequently, we can employ the small distance approximation in equation (B13) for all r_{ij}, and equation (B3) becomes

$$S_1 \simeq \frac{N}{\sqrt{\pi}R_{\rm eff}} + \sum_{\substack{i,j=1 \\ i\neq j}}^{N} \frac{1}{\sqrt{\pi}R_{\rm eff}}, \tag{B23}$$

where there are $N(N-1)$ terms in the sum. This gives

$$S_1 \simeq \frac{N^2}{\sqrt{\pi}R_{\rm eff}}, \tag{B24}$$

whose behaviour with respect to $R_{\rm eff}$ is the same in the entire interval.

B.1.4. Fourth interval: $d \leqslant R_{eff}$

For the last interval, similar considerations are applied and the terms of the sum are approximated to their small distance limit. Consequently, we obtain

$$S_1 \simeq \frac{N^2}{\sqrt{\pi}R_{\rm eff}}, \tag{B25}$$

exactly as in the third interval.

B.2. Analytical estimation of the second contribution to the sum S_2

For the second contribution to the sum (cf equation (B1)), one needs to compare $R_{\rm eff}$ with $|\mathbf{d} + \mathbf{r}_{ij}|$. Considering that $\mathbf{d}$ is orthogonal to one of the sides of the cubic lattice, we have the following bounds on $|\mathbf{d} + \mathbf{r}_{ij}|$:

$$d - L \leqslant |\mathbf{d} + \mathbf{r}_{ij}| \leqslant \sqrt{(d+L)^2 + L^2} \leqslant d + 2L, \tag{B26}$$

The second contribution is analysed in three different intervals of interest: $R_{\rm eff} \leqslant (d-L)/2$, $(d-L)/2 \leqslant R_{\rm eff} \leqslant (d+2L)/2$ and $(d+2L)/2 \leqslant R_{\rm eff}$.

B.2.1. First interval: $R_{eff} \leqslant (d-L)/2$
In this interval, we have $R_{\rm eff} \leqslant (d-L)/2 \leqslant |\mathbf{d}+\mathbf{r}_{ij}|/2$. Thus, we can safely apply the long distance approximation in equation (B13) to S_2 in equation (B1), thus obtaining

$$S_2 \simeq \sum_{i,j=1}^{N} \frac{1}{|\mathbf{d}+\mathbf{r}_{ij}|}. \tag{B27}$$

By applying the bounds in equation (B26), we can derive an upper and lower bound to S_2, which read

$$\frac{N^2}{d+2L} \leqslant S_2 \leqslant \frac{N^2}{d-L}, \tag{B28}$$

where the N^2 factor follows trivially.

B.2.2. Second interval: $(d-L)/2 \leqslant R_{eff} \leqslant (d+2L)/2$
In the second interval, $(d-L)/2 \leqslant R_{\rm eff} \leqslant (d+2L)/2$. Thus, by combining the definition of the interval with equation (B26), we obtain

$$\frac{d-L}{d+2L} \leqslant \frac{|\mathbf{d}+\mathbf{r}_{ij}|}{2R_{\rm eff}} \leqslant \frac{d+2L}{d-L}. \tag{B29}$$

Since the terms of the sum in S_2 are monotonically decreasing with respect to $\frac{|\mathbf{d}+\mathbf{r}_{ij}|}{2R_{\rm eff}}$, for each of them we have

$$\frac{1}{2R_{\rm eff}} \frac{\mathrm{erf}\left(\frac{d+2L}{d-L}\right)}{\frac{d+2L}{d-L}} \leqslant \frac{\mathrm{erf}\left(\frac{|\mathbf{d}+\mathbf{r}_{ij}|}{2R_{\rm eff}}\right)}{|\mathbf{d}+\mathbf{r}_{ij}|} \leqslant \frac{1}{2R_{\rm eff}} \frac{\mathrm{erf}\left(\frac{d-L}{d+2L}\right)}{\frac{d-L}{d+2L}}. \tag{B30}$$

It follows that

$$\frac{\epsilon_- N^2}{2R_{\rm eff}} \leqslant S_2 \leqslant \frac{\epsilon_+ N^2}{2R_{\rm eff}}, \tag{B31}$$

where

$$\epsilon_\pm = \frac{\mathrm{erf}\left[\left(\frac{d-L}{d+2L}\right)^{\pm 1}\right]}{\left(\frac{d-L}{d+2L}\right)^{\pm 1}}, \tag{B32}$$

which can be quantified once fixed the ratio between L and d. For example, for $d = 4L$, we have $\epsilon_- \simeq 0.5$ and $\epsilon_+ \simeq 1$.

B.2.3. Third interval: $(d+2L)/2 \leqslant R_{eff}$
In this interval, $R_{\rm eff} \geqslant (d+2L)/2 \geqslant |\mathbf{d}+\mathbf{r}_{ij}|/2$. So we can apply the short distance approximation in equation (B13), which trivially gives

$$S_2 \simeq \frac{N^2}{\sqrt{\pi} R_{\rm eff}}. \tag{B33}$$

B.3. Both contributions

The sum of the two contributions to $\Delta E(\mathbf{d}) = 8\pi G m^2 (S_1 - S_2)$ can be computed case by case depending on the value of $R_{\rm eff}$ compared to the other lengths involved. There are a total of six different intervals. Notably, when bounds are involved, one should account that $\min(\Delta E(\mathbf{d})) = 8\pi G m^2 (\min(S_1) - \max(S_2))$ and $\max(\Delta E(\mathbf{d})) = 8\pi G m^2 (\max(S_1) - \min(S_2))$. The intervals and the corresponding equations to be used are reported in table 1. In particular, for $(d+2L)/2 \leqslant R_{\rm eff} \leqslant d$ and $d \leqslant R_{\rm eff}$, we have that the dominant contributions cancel, namely $S_1 - S_2 \simeq 0$. For these intervals, one needs to consider also second order terms of the expansion. These give

$$\Delta E(\mathbf{d}) \simeq 8\pi G m^2 \sum_{i,j=1}^{N} \left(-\frac{r_{ij}^2}{12\sqrt{\pi} R_{\rm eff}^3} + \frac{|\mathbf{d}+\mathbf{r}_{ij}|^2}{12\sqrt{\pi} R_{\rm eff}^3} \right) = \frac{2}{3}\sqrt{\pi} G m^2 \sum_{i,j=1}^{N} \frac{d^2 + 2\,\mathbf{r}_{ij}\cdot\mathbf{d}}{R_{\rm eff}^3}. \tag{B34}$$

Table 1. Summary of the results of the analytical study of the $R_{\rm eff}$ dependence of $\Delta E(\mathbf{d})$ for different values of $R_{\rm eff}$.

Interval for $R_{\rm eff}$	Value or bounds on $\Delta E(\mathbf{d})/(8\pi Gm^2) = S_1 - S_2 = \Delta S$
$R_{\rm eff} \leqslant a$	$\frac{N}{\sqrt{\pi}R_{\rm eff}} + \frac{\eta_- N\sqrt{N}}{a} - \frac{N^2}{d-L} \leqslant \Delta S \leqslant \frac{N}{\sqrt{\pi}R_{\rm eff}} + \frac{\eta_+ N\sqrt{N}}{a} - \frac{N^2}{d+L}$
$a \leqslant R_{\rm eff} \leqslant L$	$\frac{N}{\sqrt{\pi}R_{\rm eff}} + \frac{\eta_- N\sqrt{N}}{a} - \frac{N^2}{d-L} + \frac{4NR_{\rm eff}}{\sqrt{\pi}a^2} - \frac{2\pi N}{a}\mathcal{F}_G\left(\frac{2R_{\rm eff}}{a} - 1\right) \leqslant$ $\Delta S \leqslant \frac{N}{\sqrt{\pi}R_{\rm eff}} + \frac{\eta_+ N\sqrt{N}}{a} - \frac{N^2}{d+L} + \frac{4NR_{\rm eff}}{a^2}\left(\frac{1}{\sqrt{\pi}} - 1\right)$
$L \leqslant R_{\rm eff} \leqslant \frac{(d-L)}{2}$	$\frac{N^2}{\sqrt{\pi}R_{\rm eff}} - \frac{N^2}{d-L} \leqslant \Delta S \leqslant \frac{N^2}{\sqrt{\pi}R_{\rm eff}} - \frac{N^2}{d+2L}$
$\frac{(d-L)}{2} \leqslant R_{\rm eff} \leqslant \frac{(d+2L)}{2}$	$\frac{N^2}{\sqrt{\pi}R_{\rm eff}} - \frac{\epsilon_+ N^2}{2R_{\rm eff}} \leqslant \Delta S \leqslant \frac{N^2}{\sqrt{\pi}R_{\rm eff}} - \frac{\epsilon_- N^2}{2R_{\rm eff}}$
$\frac{(d+2L)}{2} \leqslant R_{\rm eff} \leqslant d$	$\Delta S = \frac{N^2 d^2}{12\sqrt{\pi}R_{\rm eff}^3}$
$d \leqslant R_{\rm eff}$	$\Delta S = \frac{N^2 d^2}{12\sqrt{\pi}R_{\rm eff}^3}$

However, since $\mathbf{r}_{ij} = -\mathbf{r}_{ji}$ for all i and j, then $\sum_{i,j=1}^{N}\mathbf{r}_{ij} = 0$, and one obtains

$$\Delta E(\mathbf{d}) \simeq \frac{2}{3}\sqrt{\pi}Gm^2N^2\frac{d^2}{R_{\rm eff}^3}. \tag{B35}$$

Table 1 summarises the analytical study of $\Delta E(\mathbf{d})$, which is graphically reported in figure 4 where it was compared with the numerical evaluation of the sum. Finally, a last comment is due: $\Delta E(\mathbf{d})$ is a monotonically decreasing function of $R_{\rm eff}$, and this can be employed to estimate its values in those intervals where an analytical estimation is hard to be obtained. In particular, we exploited this for $R_{\rm eff}$ just below L and around $(d-L)/2$, to approximate the behaviour of $\Delta E(\mathbf{d})$ with the black dashed line in figure 4.

Appendix C. Plateau dependence on the dimensionality

Here, we quantify the dimensionality dependence of the plateau of $\tau(\mathbf{d})$, and thus $\Delta E(\mathbf{d})$, for $R_{\rm eff} \sim a$. For the sake of simplicity, we assume our system to be a sphere in $D \geqslant 2$ dimensions. Namely, this corresponds to a disk for $D = 2$ and a sphere for $D = 3$ both of radius $L/2$. For $R_{\rm eff} \sim a$, S_2 can be safely bounded with equation (B28), which is independent from the dimensionality of the problem and from $R_{\rm eff}$ as expected for the plateau. Conversely, from equation (B3) we have

$$S_1 = \frac{N}{\sqrt{\pi}a} + \sum_{\substack{i,j=1\\ i\neq j}}^{N}\frac{\mathrm{erf}\left(\frac{r_{ij}}{2a}\right)}{r_{ij}}. \tag{C1}$$

Since, independently from the dimensionality of the problem, equation (B5) still holds, one only needs to evaluate

$$\sum_{\substack{i,j=1\\ i\neq j}}^{N}\frac{1}{r_{ij}} = \sum_{\substack{i,j=1\\ i\neq j}}^{N}\frac{1}{a\left(\sum_{k=1}^{D}\left(n_k^i - n_k^j\right)^2\right)^{\frac{1}{2}}}. \tag{C2}$$

By following the reasoning described above, we estimate the latter with its upper bound (see equation (B7), which provided a very good estimate for S_1 for $R_{\rm eff} \simeq a$):

$$\sum_{\substack{i,j=1\\ i\neq j}}^{N}\frac{1}{r_{ij}} \lesssim \frac{N}{a}\sum_{\left\{n_k^j\right\}_{k=1}^{D}\in S_D}\frac{1}{\left(\sum_{k=1}^{D}\left(n_k^j\right)^2\right)^{\frac{1}{2}}}. \tag{C3}$$

This is the generalization of equation (B7) to D dimensions, with $S_D = \{n_k^j \mid 0 < |a(n_1^j, \ldots, n_D^j)| < L/2\}$ identifying a D-dimensional sphere on which the lattice is defined. Such an expression can be simply approximated to a $1/r$ integral in D dimensions, i.e.

$$\frac{N}{a}\Omega_D\int_0^{N_D/2}\mathrm{d}x\,x^{D-1}\frac{1}{x} = \frac{N}{a}\frac{2\pi^{D/2}}{\Gamma(D/2)}\frac{N^{\frac{D-1}{D}}}{2^{D-1}(D-1)}, \tag{C4}$$

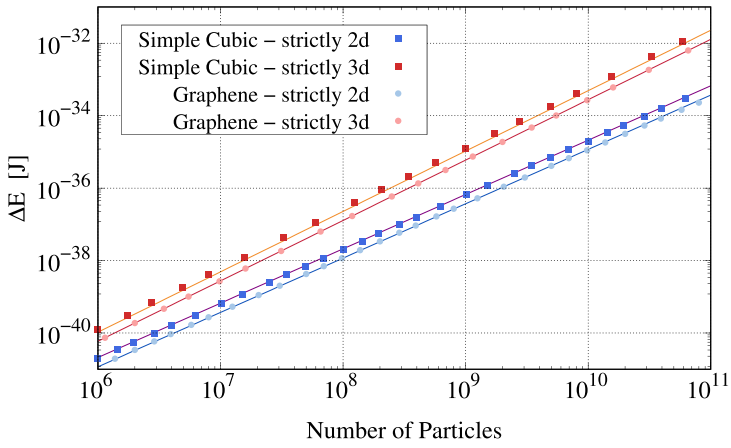

Figure 5. ΔE as a function of N for different two- and three-dimensional systems and comparison with the analytical behaviours. We numerically computed and compared the two- and three-dimensional cases. For the two-dimensional case, we took a sheet of graphene (blue dots) and a sheet of a material with a simple cubic lattice (blue squares). For the three dimensional case, we considered a cubic stack of graphene sheets (red dots) and a cube of material with a simple cubic lattice (red squares). The corresponding lines are obtained from equation (C5) for the simple cubic lattice, while are instead fitted for the case of graphene with the same dependence from N as in equation (C5). The values of the parameters are: $a = 1.0$ Å, $d = 5 \times 10^6$ Å and $m = 2.0 \times 10^{-26}$ kg for the simple cubic data and $d = 1 \times 10^6$ Å for the graphene one. In all cases, we fixed $R_{\text{eff}} = 1$ Å.

where $\Omega_D = 2\pi^{D/2}/\Gamma(D/2)$ is the D-dimensional full angle. Correspondingly, for $R_{\text{eff}} \simeq a$, one obtains

$$\Delta E(\mathbf{d}) \simeq \frac{8\pi G m^2}{a} \frac{\pi^{D/2}}{\Gamma(D/2)} \frac{N^{\frac{2D-1}{D}}}{2^{D-2}(D-1)}, \tag{C5}$$

which is plotted in figure 5 with the black and orange lines for $D = 3$ and $D = 2$ dimensions respectively. For comparison, we report the numerical estimations of $\Delta E(\mathbf{d})$.

Appendix D. Algorithm for the numerical calculation

The evaluation of equation (6) involves the calculation of the term

$$\sum_{i=1}^{N}\sum_{j=1}^{N} f(\mathbf{r}_{ij}, R_0, \mathbf{d}), \tag{D1}$$

where i and j run across all the N lattice sites and $f(\mathbf{r}_{ij}, R_0, \mathbf{d})$ is a function that depends on the distance $\mathbf{r}_{ij}$ between the sites i and j. In this form, the evaluation of equation (D1) requires the sum of N^2 terms. Given the large systems considered in this work ($N \sim 10^{10}$), a direct evaluation of this sum is not feasible on a personal computer or even on a dedicated computer facility. However, since the summed terms in equation (D1) depend only on the distance between the sites, we can rewrite such an equation as a single weighted sum across the lattice sites

$$\sum_{i=1}^{N}\sum_{j=1}^{N} f(\mathbf{r}_{ij}, R_0, \mathbf{d}) = \sum_{\mathbf{r}\in\mathcal{D}} \omega(\mathbf{r}) f(\mathbf{r}, R_0, \mathbf{d}), \tag{D2}$$

where $\mathcal{D}$ is the set of every possible distances $\mathbf{r}$ between the lattice sites, and the weight $\omega(\mathbf{r})$ is the number of pairs of lattice cells that are at a distance $\mathbf{r}$ apart.

We consider a general two-dimensional lattice, with primitive vectors $\mathbf{a}_1$ and $\mathbf{a}_2$, and basis $\mathbf{b}_\alpha$, with $\alpha = 1, \ldots, K$ being the index of the particles in the unit cell. For instance, the graphene is a two-dimensional lattice (see figure 6) with primitive vectors $\mathbf{a}_1 = a(1,0)$, $\mathbf{a}_2 = a(\frac{1}{2}, \frac{\sqrt{3}}{2})$, and basis $\mathbf{b}_1 = (0,0)$, $\mathbf{b}_2 = a(\frac{1}{2}, \frac{\sqrt{3}}{6})$, where $a = 2.46$ Å is the lattice step [48]. Each site of the lattice can be written as a linear combination of the primitive vectors with integer coefficients, $\mathbf{x}_{i,\alpha} = n_1^i \mathbf{a}_1 + n_2^i \mathbf{a}_2 + \mathbf{b}_\alpha$, with $n_1^i, n_2^i \in \mathbb{Z}$. Therefore, also the distance between two sites can be written as a linear combination of the primitive vectors. Namely

$$\mathbf{r}_{ij\alpha\beta} = \mathbf{x}_{i,\alpha} - \mathbf{x}_{j,\beta} = n_1^{ij}\mathbf{a}_1 + n_2^{ij}\mathbf{a}_2 + \mathbf{b}_{\alpha\beta}, \qquad \text{with} \quad n_1^{ij}, n_2^{ij} \in \mathbb{Z}, \tag{D3}$$

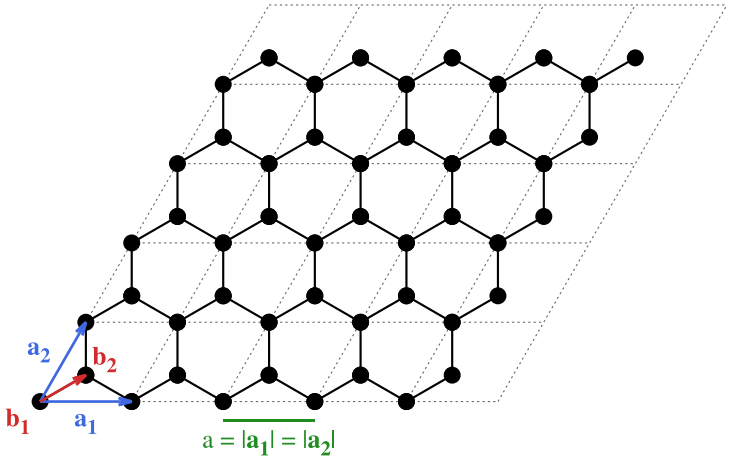

Figure 6. Graphical representation of the graphene lattice that was employed for the numerical summation. The lattice vectors are $\mathbf{a}_1 = a(1,0)$ and $\mathbf{a}_2 = a(\frac{1}{2}, \frac{\sqrt{3}}{6})$. For each cell, we have two carbon atoms, which are identified by $\mathbf{b}_1 = (0,0)$ and $\mathbf{b}_2 = a(\frac{1}{2}, \frac{\sqrt{3}}{6})$.

where $n_1^{ij} = n_1^i - n_1^j$, $n_2^{ij} = n_2^i - n_2^j$ and $\mathbf{b}_{\alpha\beta} = \mathbf{b}_\alpha - \mathbf{b}_\beta$. Then, the distance between two lattice sites can be written as a function of two integers $n_1 = n_1^{ij}$, $n_2 = n_2^{ij}$ and a vector $\mathbf{c}_\gamma = \mathbf{b}_{\alpha\beta}$. Namely, we have

$$\mathbf{r}(n_1, n_2, \gamma) = n_1\mathbf{a}_1 + n_2\mathbf{a}_2 + \mathbf{c}_\gamma, \tag{D4}$$

with $n_1, n_2 \in \mathbb{Z}$ and

$$\mathbf{c}_\gamma \in \mathcal{D}_b = \{\mathbf{b}_\alpha - \mathbf{b}_\beta \mid \alpha, \beta = 1, \ldots, K\}. \tag{D5}$$

Suppose that the lattice is finite, with N_1 and N_2 cells along the first and the second primitive vectors, respectively. In this case, the coefficients for the position of the ith site are $n_1^i \in [0, N_1 - 1]$ and $n_2^i \in [0, N_2 - 1]$. Similarly, the coefficients that define the distance between the sites are $n_1^{ij} = (n_1^i - n_1^j) \in [-N_1 + 1, N_1 - 1]$ and $n_2^{ij} = (n_2^i - n_2^j) \in [-N_2 + 1, N_2 - 1]$. As a result, the set of all possible distances between the lattice sites is

$$\mathcal{D} = \{\mathbf{r}(n_1, n_2, \gamma) \mid n_i \in [-N_i + 1, N_i - 1], \mathbf{c}_\gamma \in \mathcal{D}_b\}, \tag{D6}$$

where the form of $\mathbf{r}(n_1, n_2, \gamma)$ is defined in equation (D4).

The weights $\omega(\mathbf{r})$ are given by the number of pairs of lattice cells connected by the vector $\mathbf{r}$. The explicit value can be computed by accounting that the distance $\mathbf{r}(n_1, n_2, \gamma)$ links two cells that are separated by $n_i\mathbf{a}_i$ along the ith direction. Since the lattice is finite, there are $N_i - |n_i|$ pairs of cells at such separation. Therefore, we have

$$\omega(n_1, n_2, \gamma) = \omega_\gamma (N_1 - |n_1|)(N_2 - |n_2|), \tag{D7}$$

where ω_γ is the number of pairs of atoms in the same cell that are $\mathbf{c}_\gamma$ apart. For example, for a lattice with a single atom per unit cell there is only one basis vector $\mathbf{b}_1 = (0,0)$ and only one possible (null) distance between atoms in the same cell. Thus, $\mathcal{D}_b = \{\mathbf{c}_1 = (0,0)\}$ and $\omega_1 = 1$. Conversely, for the graphene plate, which is the case of interest, one has $\mathbf{b}_1 = (0,0)$ and $\mathbf{b}_2 = a(\frac{1}{2}, \frac{\sqrt{3}}{6})$. According to equation (D5), we have

$$\begin{aligned} \mathcal{D}_b &= \{\mathbf{c}_1 = \mathbf{b}_1 - \mathbf{b}_1, \mathbf{c}_2 = \mathbf{b}_1 - \mathbf{b}_2, \mathbf{c}_3 = \mathbf{b}_2 - \mathbf{b}_1, \mathbf{c}_4 = \mathbf{b}_2 - \mathbf{b}_2\}, \\ &= \left\{\mathbf{c}_1 = (0,0), \mathbf{c}_2 = -a\left(\tfrac{1}{2}, \tfrac{\sqrt{3}}{6}\right), \mathbf{c}_3 = a\left(\tfrac{1}{2}, \tfrac{\sqrt{3}}{6}\right), \mathbf{c}_4 = (0,0)\right\}. \end{aligned} \tag{D8}$$

Since $\mathbf{c}_4 = \mathbf{c}_1$, we can neglect $\mathbf{c}_4$ and count twice $\mathbf{c}_1$. Then, we find $\omega_1 = 2$ and $\omega_2 = \omega_3 = 1$.

By considering the explicit form of the weights, equation (D2) becomes

$$\sum_{\mathbf{r}\in\mathcal{D}} \omega(\mathbf{r}) f(\mathbf{r}, R_0, \mathbf{d}) = \sum_{n_1=-N_1+1}^{N_1-1} \sum_{n_2=-N_2+1}^{N_2-1} \sum_{\mathbf{c}_\gamma \in \mathcal{D}_b} \omega_\gamma (N_1 - |n_1|)(N_2 - |n_2|) f(\mathbf{r}(n_1, n_2, \gamma), R_0, \mathbf{d}). \tag{D9}$$

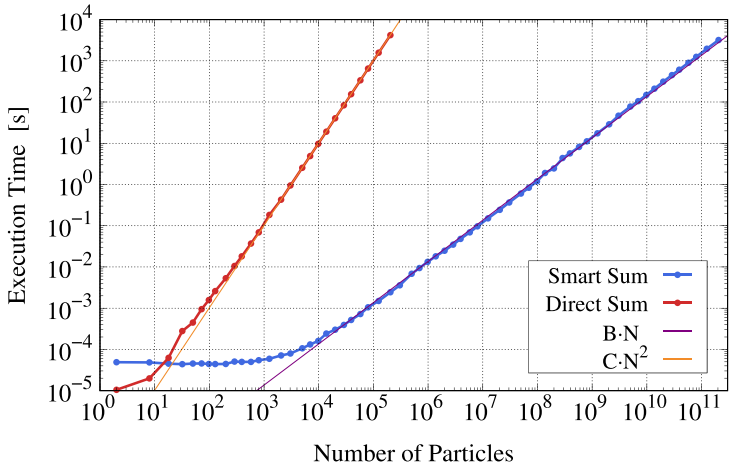

Figure 7. Execution time for the numerical summation as a function of the number of particles N for a plate of graphene. Each point corresponds to a single evaluation equations (D10) (blue dots and fitted line) and (D1) (red dots and fitted line). The purple and orange lines provide the scaling laws for equations (D10) and (D1) respectively.

Such an expression involves the sum of

$$(2N_1-1)(2N_2-1)[1+K(K-1)] \simeq 4N_1N_2[1+K(K-1)] = 4\frac{[1+K(K-1)]}{K}N \tag{D10}$$

terms, where we used that the total number of atoms is given by the product of the number of cells per direction times the number of atoms per cell, i.e. $N = N_1N_2K$. These expressions are valid for any two-dimensional lattice, but can be easily generalized to higher dimensions.

As shown by equation (D10), the sum involves a number of terms that scales linearly with the number of atoms. Such a scaling needs to be compared with the quadratic one provided by equation (D1). Correspondingly, we obtain a speedup in the numerical summation for $N \gtrsim 20$, which reaches a factor of 10^{10} for $N \sim 10^{10}$. Figure 7 provides the comparison of the execution time for the numerical summation when employing equations (D10) (blue dots) and (D1) (red dots), for $R_0 = 1\,\text{Å}$ and $d = 10^6\,\text{Å}$. For the summation we employed a simple in-house python code with `numba` just-in-time compiler [49] on a personal laptop with Intel processor i7-8750 H. We extensively verified that the results of the two sums coincide to the same value, up to the machine precision for system with $N \leqslant 2 \times 10^5$ particles. Moreover, when we evaluated equation (D1) for very large systems and $d \lesssim a$, we found that the accumulation of rounding errors produced an overall error that can reach the order of magnitude of the entire sum, thus making the estimation of the sum worthless.

ORCID iDs

Laria Figurato https://orcid.org/0000-0002-2225-0655
Matteo Carlesso https://orcid.org/0000-0002-9929-7291
Angelo Bassi https://orcid.org/0000-0001-7500-387X

References

[1] DeWitt B S 1967 *Phys. Rev.* **160** 1113
[2] Diósi L 1984 *Phys. Lett.* A **105** 199
[3] Hooft G 1993 arXiv:gr-qc/9310026
[4] Rovelli C 1998 *Living Rev. Relativ.* **1** 1
[5] Green M B, Schwarz J H and Witten E 2012 *Superstring Theory: Volume 2, Loop Amplitudes, Anomalies and Phenomenology* (Cambridge University Press)
[6] Adler S 2016 *Gravitation and the Noise Needed in Objective Reduction Models* (*Quantum Nonlocality and Reality: 50 Years of Bell's Theorem*) ed M Bell and S Gao (Cambridge University Press)
[7] Karolyhazy F 1966 *Il Nuovo Cimento* A **42** 390
[8] Ellis J, Hagelin J S, Nanopoulos D V and Srednicki M 1984 *Nucl. Phys.* B **241** 381
[9] Kafri D, Taylor J and Milburn G 2014 *New J. Phys.* **16** 065020
[10] Tilloy A and Diósi L 2016 *Phys. Rev.* D **93** 024026
[11] Bassi A, Großardt A and Ulbricht H 2017 *Class. Quantum Grav.* **34** 193002
[12] Oppenheim J, Sparaciari C, Šoda B and Weller-Davies Z 2023 *Nat. Commun.* **14** 7910
[13] Oppenheim J 2023 *Phys. Rev.* X **13** 041040

[14] Bell J S 2004 *Speakable and Unspeakable in Quantum Mechanics: Collected Papers on Quantum Philosophy* (Cambridge University Press)
[15] Diósi L 1987 *Phys. Lett.* A **120** 377
[16] Diósi L 1989 *Phys. Rev.* A **40** 1165
[17] Penrose R 1996 *Gen. Relativ. Gravit.* **28** 581–600
[18] Penrose R 2000 Wavefunction collapse as a real gravitational effect *Mathematical Physics* (Imperial College Press) pp 266–82
[19] Penrose R 2014 *Found. Phys.* **44** 557
[20] Bahrami M, Smirne A and Bassi A 2014 *Phys. Rev.* A **90** 062105
[21] Howl R, Penrose R and Fuentes I 2019 *New J. Phys.* **21** 043047
[22] Di Bartolomeo G, Carlesso M, Piscicchia K, Curceanu C, Derakhshani M and Diósi L 2023 *Phys. Rev.* A **108** 012202
[23] Di Bartolomeo G and Carlesso M 2024 *New J. Phys.* **26** 043006
[24] Tomaz A A, Mattos R S and Barbatti M 2024 *Phys. Chem. Chem. Phys.* **26** 20785
[25] Ghirardi G C, Rimini A and Weber T 1986 *Phys. Rev.* D **34** 470
[26] Ghirardi G C, Pearle P and Rimini A 1990 *Phys. Rev.* A **42** 78
[27] Bassi A and Ghirardi G 2003 *Phys. Rep.* **379** 257
[28] Bassi A, Lochan K, Satin S, Singh T P and Ulbricht H 2013 *Rev. Mod. Phys.* **85** 471
[29] Carlesso M, Donadi S, Ferialdi L, Paternostro M, Ulbricht H and Bassi A 2022 *Nat. Phys.* **18** 243
[30] Toroš M and Bassi A 2018 *J. Phys. A: Math. Theor.* **51** 115302
[31] Tilloy A and Stace T M 2019 *Phys. Rev. Lett.* **123** 080402
[32] Helou B, Slagmolen B, McClelland D E and Chen Y 2017 *Phys. Rev.* D **95** 084054
[33] Vinante A and Ulbricht H 2021 *AVS Quantum Sci.* **3** 045602
[34] Donadi S, Piscicchia K, Curceanu C, Diósi L, Laubenstein M and Bassi A 2021 *Nat. Phys.* **17** 74
[35] Arnquist I *et al* 2022 *Phys. Rev. Lett.* **129** 080401
[36] Ghirardi G, Grassi R and Rimini A 1990 *Phys. Rev.* A **42** 1057
[37] Blake P, Hill E, Castro Neto A, Novoselov K, Jiang D, Yang R, Booth T and Geim A 2007 *Appl. Phys. Lett.* **91** 063124
[38] Jacobs G H 2003 *Comparative Psychology of Vision* (Wiley Online Library)
[39] Marshall W, Simon C, Penrose R and Bouwmeester D 2003 *Phys. Rev. Lett.* **91** 130401
[40] Diósi L and Strunz W T 199 *Phys. Lett.* A **235** 569
[41] Bassi A and Ghirardi G 2002 *Phys. Rev.* A **65** 042114
[42] Adler S L and Bassi A 2007 *J. Phys. A: Math. Theor.* **40** 15083
[43] Bassi A and Ferialdi L 2009 *Phys. Rev.* A **80** 012116
[44] Carlesso M, Ferialdi L and Bassi A 2018 *Eur. Phys. J.* D **72** 1
[45] Piscicchia K, Donadi S, Manti S, Bassi A, Derakhshani M, Diósi L and Curceanu C 2024 *Phys. Rev. Lett.* **132** 250203
[46] Savage C M and Walls D F 1985 *Phys. Rev.* A **32** 2316
[47] Smirne A and Vacchini B 2010 *Phys. Rev.* A **82** 042111
[48] Yang G, Li L, Lee W B and Ng M C 2018 *Sci. Technol. Adv. Mater.* **19** 613
[49] Lam S K, Pitrou A and Seibert S 2015 *Proc. Second Workshop on the LLVM Compiler Infrastructure in HPC* (*Association for Computing Machinery*) pp 1–6